1 September 2000

ELSEVIER

Chemical Physics Letters 327 (2000) 76–84

CHEMICAL PHYSICS LETTERS

www.elsevier.nl/locate/cplett

A reflection principle for the control of molecular photodissociation in solids: model simulation for F_2 in Ar

R. Benny Gerber [a], Mikhail V. Korolkov [b,c,*], Jörn Manz [c], Masha Y. Niv [a], Burkhard Schmidt [d]

[a] *Hebrew University, Fritz-Haber-Center for Molecular Dynamics, Givat Ram, 91904 Jerusalem, Israel*
[b] *National Academy of Sciences of Belarus, Institute of Physics, Skaryna Avenue 70, 220602 Minsk, Belarus*
[c] *Freie Universität Berlin, Institut für Physikalische und Theoretische Chemie, Takustrasse 3, D-14195 Berlin, Germany*
[d] *Freie Universität Berlin, Institut für Mathematik, Arnimallee 2-6, D-14195 Berlin, Germany*

Received 2 May 2000

Abstract

Laser pulse-induced photodissociation of molecules in rare-gas solids is investigated by representative quantum wavepackets or classical trajectories which are directed towards, or away from, cage exits, yielding dominant photodissociation into different neighbouring cages. The directionality is determined by a sequence of reflections inside the relief provided by the slopes of the potential energy surface of the excited system, which in turn depend on the initial preparation of the matrix isolated system, e.g. by laser pulses with different frequencies or by vibrational pre-excitation of the cage atoms. This reflection principle is demonstrated for a simple, two-dimensional model of F_2 in Ar.

1. Introduction

The yield and product specificity of molecular photodissociation may be determined by means of several variants of the reflection principle [1]. For example, in the simple case of direct photodissociation of a diatomic molecule, the initial wavepacket of the reactant is excited vertically from the potential energy surface (PES) V_g of the electronic ground state to the repulsive PES V_e of the electronic excited state, according to the Franck–Condon principle. The repulsive V_e then acts as a 'mirror', e.g. different lobes of the initial wavepacket ψ_g are excited to different domains of V_e with high or low potential energies, from where they are reflected towards products with high or low translational energies, respectively. As a consequence, the shape of ψ_g is mapped onto the product kinetic energy distribution. For example, a reactant which has been pre-excited to the vth vibrational state has a wavefunction with v nodes, and this is reflected into a multi-(v)-nodal product energy distribution. Analogous reflection principles apply to photodissociation of vibrationally pre-excited polyatomic molecules [2]. In particular, pre-excitation of bending vibrations can be converted into specific rotational product excitations [1].

In this Letter, we extend the reflection principle from photodissociation of a diatomic molecule in the gas phase to the solid assuming rigid pre-orientation

* Corresponding author. E-mail: korolkov@chemie.fu-berlin.de

0009-2614/00/$ - see front matter
PII: S0009-2614(00)00799-5

of the matrix isolated molecule. The interactions of the matrix-isolated molecule with its neighboring atoms change the simple, one-dimensional repulsive V_e of the isolated system into a rather complex multi-dimensional PES, with several minima and barriers. As a consequence, one may anticipate more complex dynamics of the representative wavefunctions or trajectories, possibly including reflections from several slopes of V_e in the solid, in comparison with just one reflection in the gas phase. These multiple reflections inside the relief of the excited state PES shall be referred to as 'relief reflection' throughout this Letter. This phenomenon is, indeed, inherent in recent simulations of photodissociation of matrix-isolated molecules [3], and also in similar simulations for molecules embedded in clusters [4–6]. Here we address a specific aspect, i.e. the effect of relief reflections on the directionality of the wavepackets, or trajectories traveling on V_e. Moreover, we investigate the possibility to use this effect for laser control of the directionality. For example, we shall consider the task of driving the wavepacket, by means of multiple reflections, towards or away from a specific cage exit to one of the neighboring cages, thus controlling the relative yield of photodissociation. A complimentary approach to laser control of photodissociation versus recombination has been suggested recently in Ref. [7,5], i.e. rotational preexcitation of the matrix isolated molecule so that the lobes of the representative wavepacket point preferably towards cage exits for photodissociation, or towards repulsive walls of the potential energy surface, respectively.

In principle, one may design various scenarios for relief reflections from the walls of potential energy surfaces, which lead to control of the directionality of the representative wavepackets or trajectories. Here we center attention on the specific purpose, i.e. directing the wavepacket, or trajectories, towards or away from cage exits. For this purpose, we consider as an example a two-dimensional model of F_2 in Ar, the realistic basis of which shall be discussed below. The advantage is that this simple model lends itself to a rather easy demonstration of the control of the directionality, in principle. Moreover, it allows complementary investigations of fully quantum versus classical simulations – this comparison may serve as a reference for analogous classical, or mixed quantum-classical applications to the system, or similar ones, in full dimensionality, i.e. where a full quantum simulation is prohibitive. The model and the techniques are in Section 2, the results and discussions in Section 3, and the conclusions in Section 4.

2. Model and techniques

The construction of our two-dimensional model of F_2 in Ar is illustrated in Fig. 1. We assume that initially $(t = 0)$ the system is centered at its equilibrium position in its electronic ground state. Specifically, the F_2 molecule is located at a mono-substitutional site of the Ar fcc lattice, with its bond oriented along the $\langle 111 \rangle$ direction, thus pointing towards two opposite cage exits for the photodissociated F-atoms. Each of these cage exits consists of three Ar-atoms forming windows in equilateral triangular configuration. All the atoms are frozen in their equilibrium positions, except for two degrees of freedom which describe the F–F distance (x), and the symmetric stretching (y) of the two windows through which

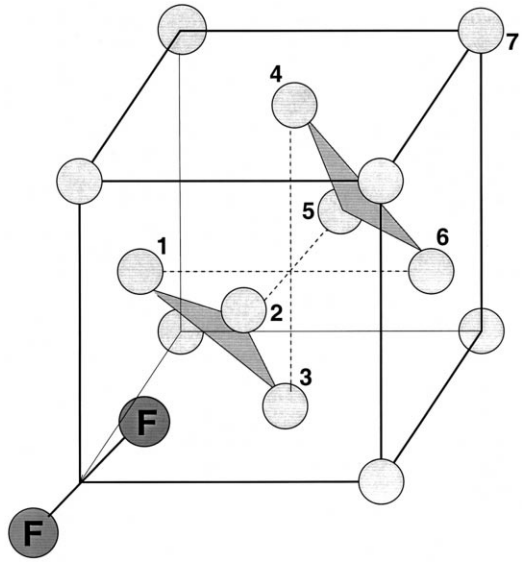

Fig. 1. Molecular fluorine occupying a monosubstitutional site in a face-centered cubic (fcc) argon crystal. The first cage exit window is the equilateral triangle (atoms 1,2,3) encountered at an F–F distance of $x \approx 11.5 a_0$. Further along the $\langle 111 \rangle$ axis there is the second window comprising of atoms 4,5,6 at $x \approx 23.0 a_0$ and finally atom 7 on the axis at $x \approx 34.4 a_0$.

cage exit may occur, i.e. the three atoms labeled 1,2,3 in Fig. 1 and another triangle obtained from the first by inversion symmetry with respect to the F–F center of mass. In quantum-mechanical representation, the corresponding initial state, which may have v_x and v_y quanta in the vibrations along x and y, respectively, is described by the eigenfunctions $\psi_{g;v_x,v_y}(x,y)$ of the ground state Hamiltonian

$$\hat{H}_g = \hat{T} + V_g\,, \tag{1}$$

where $\hat{T}$ is the kinetic energy operator for the F- and Ar-atoms comprising our two-dimensional model,

$$\hat{T} = -\frac{\hbar^2}{2m_x}\frac{\partial^2}{\partial x^2} - \frac{\hbar^2}{2m_y}\frac{\partial^2}{\partial y^2} \tag{2}$$

with reduced masses $m_x = m_F/2$ and $m_y = 6m_{Ar}$. For the calculation of the ground and excited state potential energy surfaces V_g and V_e we resort to the diatomics-in-molecule (DIM) approximation [8] which has been frequently used in molecular dynamics (MD) simulations of atomic and molecular impurities in rare-gas solids [9–12] where the Hamiltonian is constructed from atom–atom pair potentials which also depend on the orientation of the P-state atom of the open-shell F-atom in order to model the anisotropy of the electron densities. For details, the reader is referred to forthcoming papers [13,12]. Actually, a manifold of 36 electronic states is pertinent to the photodissociation of F_2 into $F(^2P) + F(^2P)$, and all the corresponding PESs are modelled by DIM. Here, for simplicity, we use a single excited electronic state in addition to the ground state, from this manifold. Ref. [13] discusses the validity of the two-dimensional model. By comparison with full-dimensional classical simulations, we find that within the first 200–300 fs (depending on the laser frequency) the (x,y) degrees of freedom indeed describe the dynamics very well. At longer timescales, however, the remaining degrees of freedom can no longer be neglected.

In summary, the reduced dimensionality of the model employed here, and the neglect of all excited electronic states but one, are serious approximations. However, at least for short timescales, the model is sufficiently realistic to be physically useful. The excitation of $\psi_{g;v_x,v_y}(x,y)$ from V_e to V_g by a laser pulse, and the subsequent time evolution of the nuclear wavepackets $\psi_g(x,y,t)$ and $\psi_e(x,y,t)$ on V_g and V_e, are described by the time-dependent Schrödinger equation

$$i\hbar\frac{\partial}{\partial t}\begin{bmatrix}\psi_g(t)\\ \psi_e(t)\end{bmatrix} = \begin{bmatrix}\hat{T}+V_g & -\mu_{ge}\mathscr{E}(t)\\ -\mu_{ge}\mathscr{E}(t) & \hat{T}+V_e\end{bmatrix}\begin{bmatrix}\psi_g(t)\\ \psi_e(t)\end{bmatrix} \tag{3}$$

where μ_{ge} is the transition dipole operator, and $\mathscr{E}$ is the electric field. For simplicity, we assume the Condon approximation, i.e. $\mathscr{E}_0\,\mu_{ge} = 0.03E_h$ is a constant, and the electric field is polarized parallel to the transition dipole moment μ_{ge},

$$\mathscr{E}(t) = \mathscr{E}_0\cos\omega t\sin^2\left(\frac{t\pi}{\tau}\right), \quad 0 \leqslant t \leqslant \tau \tag{4}$$

with carrier frequency ω, amplitude $\mathscr{E}_0$, duration τ, and $\sin^2$-like shape function. Both potential functions and wavefunctions are represented on an equidistant grid of 1024×512 points ($1.9a_0 \leqslant x \leqslant 29.1a_0$, $2.6a_0 \leqslant y \leqslant 7.2a_0$) thus allowing an exact and efficient evaluation of the kinetic operator by means of two-dimensional fast Fourier transforms (FFT). The time evolution is discretized in steps of $1–4\hbar/E_h$ and the split operator algorithm is applied [14].

Alternatively, we also carry out semiclassical simulations of the laser driven dynamics. The initial wavefunction $\psi_{g;v_x,v_y}$ is Wigner transformed [15] and sampled in a Monte Carlo fashion to yield initial values for the trajectories. The excitation process is modeled by a surface hopping scheme in close analogy to the numerical treatment of nonadiabatic effects [16] assuming the probability for the excitation of a single trajectory to be proportional to $|\mu_{ge}\mathscr{E}(t)|^2$; for details see also Ref. [13].

3. Results

Before presenting the laser-induced dynamics on the electronically excited state, let us first consider the respective PESs for our two-dimensional model. The ground state potential $V_g(x,y)$ has a deep minimum located at an equilibrium position of $x_{eq} = 2.66$

a_0 and $y_{eq} = 4.14\ a_0$. As a consequence, the initial vibrational wavefunctions $\psi_{g;v_x,v_y}(x,y)$ are well located around this point for low values of quantum numbers v_x, v_y. The excited state potential $V_e(x,y)$ is shown as a contour plot in Fig. 2. It has three potential minima labeled I,II,III, corresponding to different interstitial cages of the fcc lattice. The first minimum corresponds to an electronically excited F_2 molecule trapped in front of the first argon windows provided by the crystallografic (111) planes nearest to the guest molecule. The second and third minimum correspond to local minima for the two dissociated F-atoms separated by one or two pairs of (111) planes of the fcc lattice, respectively. The domains of these potential minima are separated by barriers indicated by vertical arrows in Fig. 2 ($x = 11.5a_0$, $x = 23.0\,a_0$). They correspond to penetration of the first and second window formed by the atoms labeled 1,2,3 and 4,5,6 in Fig. 1, respectively. The fact that the second minimum is located at a slightly larger value of y than the first and third minimum is due to the repulsive forces of the F-atoms colliding with the Ar-atoms forming the windows between the initial monosubstitutional site and the neighboring cage. The valley of the PES surrounding the path from minimum I via minimum II to minimum III has steep walls between the F-atoms at short distances or between the Ar-atoms for large values of y, or between the dissociated F-atoms and the Ar-atom labeled 7 in Fig. 1 which is located on the $\langle 111 \rangle$ axis ($x = 34.4\,a_0$). These walls have a rather complex topology, with several convex or concave bends, causing relief reflections of the wavepackets representing the dynamics of the laser excited system.

In order to demonstrate the effects of relief reflections from the V_e potential slopes on the directionality of quantum wavepackets, let us consider, exemplarily, four cases of laser pulse excitations of the model system, F_2 in Ar, from the electronic ground state to the electronic excited state. The first three cases (i),(ii), (iii) assume that initially the wavepacket is prepared in the vibrational ground state, i.e. $\psi_g(t = 0) = \psi_{g;0,0}$. The fourth case (iv) assumes vibrational pre-excitation of the Ar-atoms which form the first cage exit, specifically $\psi_g(t = 0) = \psi_{g;0,2}$. The laser pulses have the same durations, $\tau = 100$ fs, but different carrier frequencies, (i) $0.24E_h/\hbar$ (6.53 eV), (ii) $0.30E_h/\hbar$ (8.16 eV), and (iii,iv) $0.26E_h/\hbar$ (7.07 eV). The resulting time evolution of the wavepacket $\psi_e(t)$ moving on the excited state PES V_e is illustrated by representative snapshots in Figs. 2 and 4, respectively. Each snapshot shows the probability density $\rho_e(t) = |\psi_e(t)|^2$ superimposed on the contour plots of V_e. They allow the following interpretation.

In case (i), the wavepacket $\psi_e(t)$ on V_e is created by the laser pulse in the Franck–Condon domain where

$$V_e(x,y) - V_g(x,y) \approx \hbar\omega \tag{5}$$

close to the equilibrium configuration (x_{eq}, y_{eq}). This domain is labeled by 'A' in Fig. 2, i.e. it is the domain of the repulsive wall of V_e, similar to the repulsive wall of V_e for F_2 molecule in the gas phase. As a consequence, the initial ground state wavepacket $\psi_{g;0,0}$ is transformed into a wavepacket $\psi_e(t)$ which runs towards larger values of x, similar to photodissociation of the free F_2. Soon after this initial photodissociation, however, the wavepacket ψ_e approaches the domain of the repulsive forces of the neighboring Ar-atoms which form the window between the original and the neighboring cage. The dissociating F-atoms push these Ar-atoms (1,2,3) aside, thus opening the triatomic windows of the cage. This 'kick' of the F-atoms against their Ar neighbors corresponds to a reflection of the wavepacket $\psi_e(t)$ from the repulsive wall of V_e, labelled 'B' in Fig. 2 ($t = 80$ fs). Subsequently, the photodissociation continues, and the F-atoms escape through the cage exit. Shortly after this event, however, the Ar-atoms which had been pushed away during the reflection at site 'B' are repelled from their nearest Ar neighbors ($t = 150$ fs). Corresponding to another reflection of the wavepacket from the wall of V_e in the domain labeled 'C' in Fig. 2 ($t = 220$ fs), $\psi_e(t)$ is scattered back through the first cage exit towards the original cage ($t = 300$ fs) without ever penetrating through the second window (4,5,6) into the next nearest cage corresponding to the domain of minimum III in Fig. 2. On a longer time scale, the F-atoms are likely to undergo nonadiabatic transitions eventually leading to recombination. Indeed, semiclassical MD simulations that were carried out recently, show recombination events on a weakly bound excited state of F_2, as well as on the ground state [12]. It must be kept in mind that the validity of our model as a realistic description of F_2

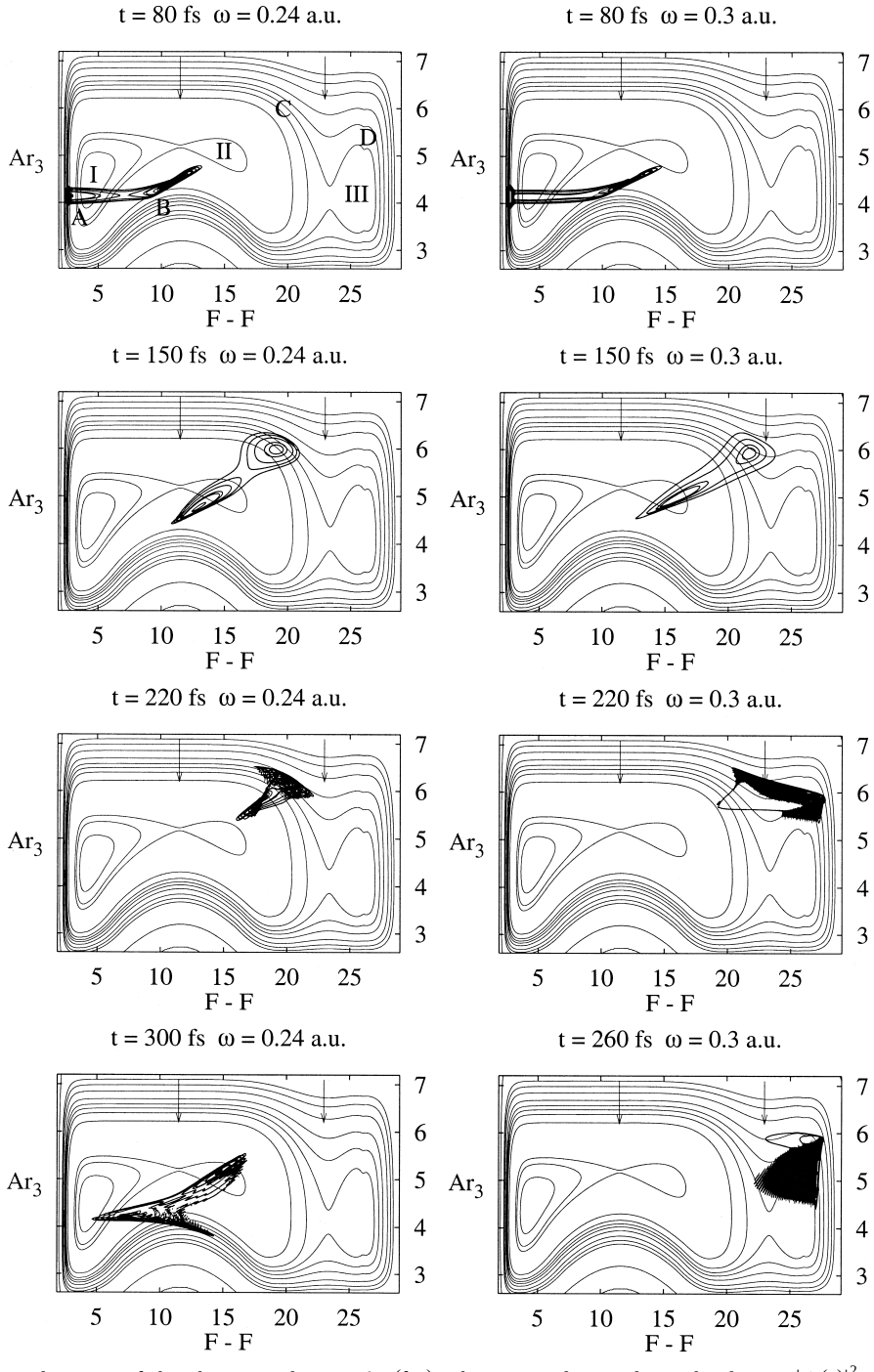

Fig. 2. Excited state dynamics of the photoexcited F_2 in Ar (fcc). The contour lines indicate the density $|\psi_e(t)|^2$ of the wavepacket superimposed on the equipotential lines of the electronically excited state. The system is excited by a $\sin^2$ shaped pulse of 100 fs duration with $\mu\mathscr{E}_0 = 0.03E_h$. Left panel: Various snapshots for a carrier frequency $\omega = 0.24E_h/\hbar$ leading mainly to trapping of the wavepacket (case i). Right panel: The same for $\omega = 0.30E_h/\hbar$ resulting in cage exit (case ii).

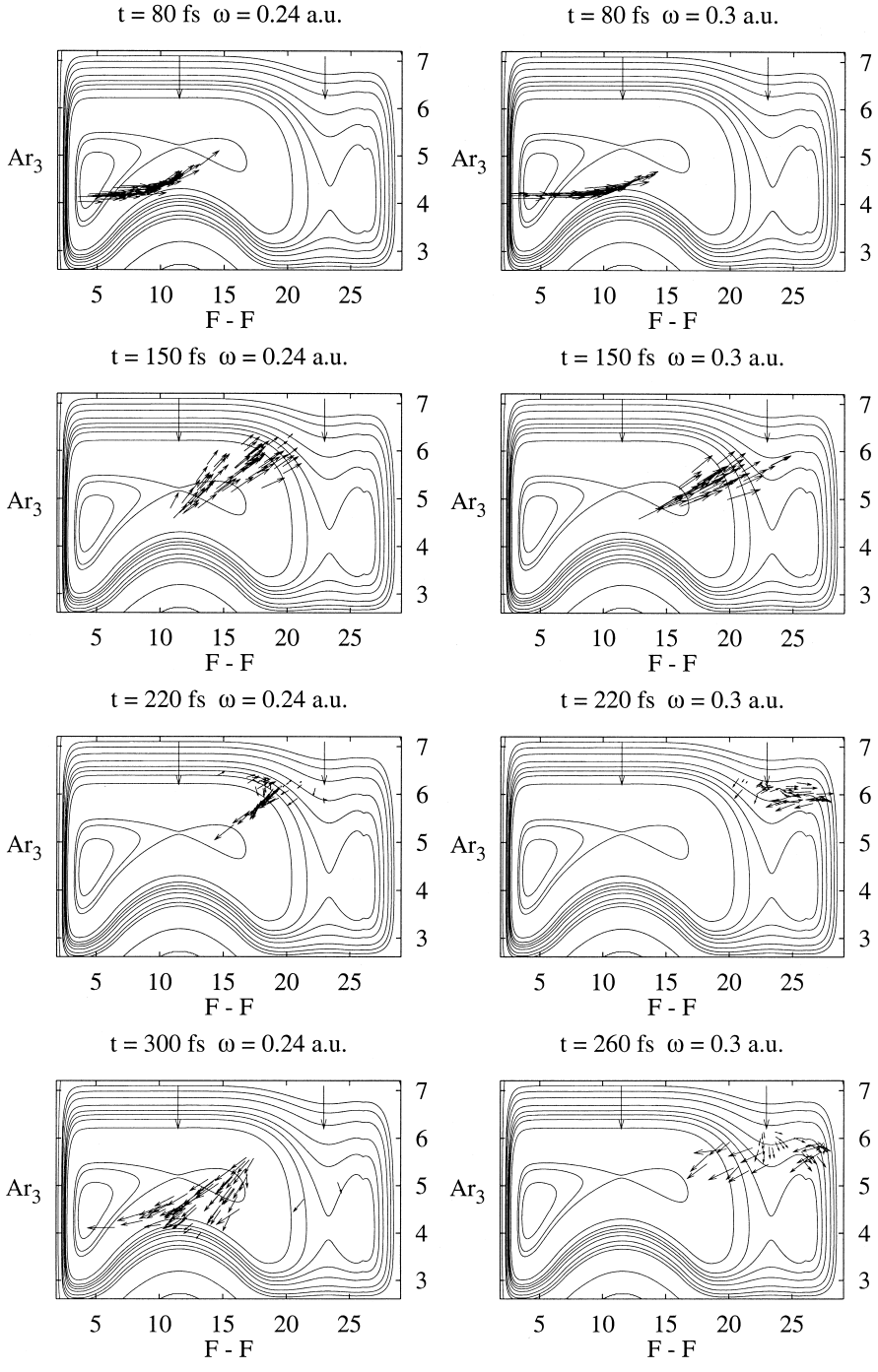

Fig. 3. Same as in Fig. 2 but the wavepacket propagation has been replaced by a quasi-classical trajectory simulation with initial values sampled from Wigner transforms of the initial wavepackets. The basis of the arrows represent the position space density, the arrowheads indicate the velocities.

in Ar is in any case restricted to very short timescale only ($t \leqslant 200$ fs or so).

In case (ii), the excited state wavepacket $\psi_e(t)$ is created in a slightly different, albeit neighboring

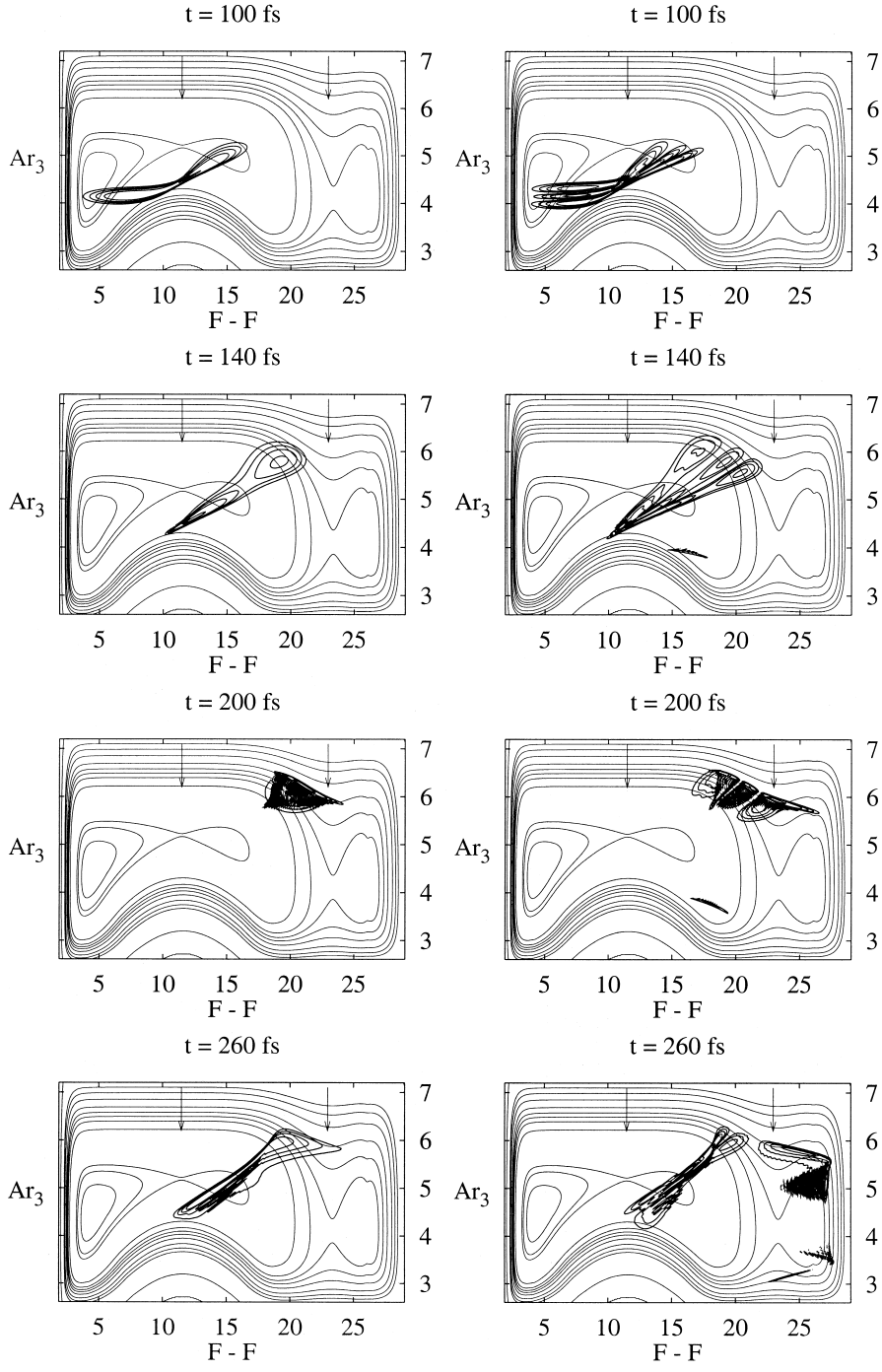

Fig. 4. Effect of vibrational pre-excitation of the Ar_3 symmetric stretching coordinate y of the first window for a carrier frequency of $\omega = 0.26 E_h/\hbar$. Left panel: Without pre-excitation (case iii). Right panel: With two quanta of vibration in the y coordinate (case iv).

Franck–Condon region, corresponding to the repulsive domain with even higher potential energy V_e than in case (i), due to the higher frequency of the exciting laser pulse, 0.30 instead of $0.24E_h/\hbar$; see Eq. (5). As a consequence, the wavepacket is no longer scattered back towards the original cage as in case (i) but it is directed through the second window (atoms 4,5,6) towards the second neighboring cage at site C ($t = 220$ fs). Later on, there it hits the steep repulsive wall (provided by atom 7) in the domain labelled D in Fig. 2 ($t = 260$ fs). Here we have reached the limit of our two-dimensional model which does not account for motion of the the second window or the atoms beyond it. However, one might speculate that in case (ii) the energy of the F-atoms dissipates into the crystal thus largely preventing recombination as in case (i).

Classical trajectory simulations corresponding to the quantum mechanical wavepacket evolution are presented in Fig. 3. Essentially, the classical simulations exhibit the same features, in particular the pattern of multiple reflections from the relief of the repulsive walls of $V_e(x,y)$ as demonstrated in the wavepacket propagations of Fig. 2.

At first glance, one might conclude that the effect demonstrated in cases (i) and (ii) is exclusively a consequence of the initial energy of the wavepacket $\psi_e(t)$ due to the different carrier frequency of the laser field, i.e. the higher the excitation energy, the more efficient the penetration of the dissociated F-atoms into the second nearest cage. This conclusion is, however, falsified by our following examples (iii) and (iv). Here we investigate the effect of vibrational pre-excitation of the Ar-atoms forming the windows of the first cage exit. Fig. 4 compares the wavepacket dynamics for a wavepacket starting from the vibrational ground state $\psi_{g;0,0}$ (case iii) with that of a wavepacket initially pre-excited to the $\psi_{g;0,2}$ state (case iv). It is emphasized that the initial energy for the two cases is practically the same since the energy difference is only $0.00046E_h$ (12.5 meV). The laser frequency for cases (iii) and (iv) is chosen to be $\omega = 0.26E_h/\hbar$ so that the total energy of the system is between that of cases (i) and (ii). In the course of the excitation process, $\psi_e(t)$ is created in the Franck–Condon domain A. The subsequent dynamics of the wavepacket starting from the vibrational ground state is depicted in the left panel of Fig. 4. Essentially, the wavepacket dynamics follows the same pattern as in case (i) ($\omega = 0.24E_h/\hbar$; see Fig. 2). The right panel of Fig. 4 shows the time evolution of the pre-excited wavepacket. It is also created in the domain A and reflected from the wall of V_e into the domain B ($t = 100$ fs). Since this wall has a concave curvature, it acts like a concave mirror mapping the three lobes of the initial wavefunction into three broader ones which are diverging ($t = 140$ fs). Only a tiny fraction of the wavepacket has enough energy to pass through B along a straight line which, however, is of not much importance here (but for even higher pre-excitation, it becomes a major pathway). Subsequently, the main part of $\psi_e(t)$ hits the opposite wall of V_e which is S-shaped, i.e. with alternating convex and concave curvature for smaller and larger values of x, respectively ($t = 200$ fs). Incidentally, the two outer lobes of $\psi_e(t)$ which correspond to wider opening of the Ar windows, are reflected at B to the concave domain of V_e close to C so that they are scattered back interferingly via the first exit of the initial cage ($t = 260$ fs). In contrast, the inner lobe of $\psi_e(t)$ which corresponds to a smaller window size is reflected from region B to the convex domain of V_e close to C thus allowing the net forward scattering into the second neighboring cage. Hence, the specific topology of V_e induces multiple scattering of $\psi_e(t)$ in the regions A, B, C which ultimately yield a complete separation of $\psi_e(t)$ – one of its three lobes is reflected towards the second cage, the others not. In summary, the comparison of cases (iii) and (iv) shows that the efficiency of cage exit versus trapping is not only determined by the initial excitation energy but rather by the specific pattern of relief reflections from the walls of the complex potential energy surface.

4. Conclusions

The present two-dimensional model simulations of the laser pulse induced photodissociation of F_2 in Ar demonstrate an extension of previous rather simple reflection principles for photodissociation of molecules in the gas phase [1,2] towards more complex, relief reflections in solids. The detail of these multiple reflections depend on subtle details such as concave and convex walls of the excited state poten-

tial energy surface V_e, and on the initial preparation of the system. Ultimately, different parts of the initial wavepacket may be directed by means of multiple reflections towards the domains of different cages for the dissociated atoms in the solid. The directionality (and not just the total energy!) is the decisive property which determines the mapping of the initial wavefunction $\psi_{g;v_x,v_y}$ on specific domains for different parts of $\psi_e(t)$. This directionality may be controlled by the initial preparation of the system, e.g. different vibrational (v_x,v_y) pre-excitation, or different laser frequencies. The present results have been derived from representative quantum wavepackets for a simple two-dimensional model. The quantum results could essentially be reproduced by corresponding classical trajectory simulations. This has encouraged us to extend the present study to classical simulations of F_2 in Ar in full dimensionality where quantum simulations are prohibitive. In particular, for longer times after the end of the laser pulse, the resulting photodissociation dynamics starts to deviate from the two-dimensional simulations. For example, trajectories which penetrate into the second cage are not always scattered back into the initial cage but they may be trapped due to dissipation of their energy to degrees of freedom not included in the simple model presented here. The details of this extended simulation will be published elsewhere [13]. Suffice it here to say that the effects of multiple reflections discovered for the low-dimensional model are also valid in full dimensionality, at least for times up to 200 fs after the end of the laser pulse. Finally, the model of directional control of photodissociation in condensed phases based on reflection of photodissociation fragments from a potential relief is a very broad one, by no means confined to the system presented here. Indeed, the choice of the model here was guided in part by ongoing experiments and consideration of experimental feasibility. By theoretical consideration photolysis of HX (X, a halide) in a heavy rare-gas solid might be promising in terms of a reduced dimensionality model. While ultrafast experiments on the scale of H-atom dynamics may not be quite available yet, it is a matter for the near future that such systems can be studied.

Acknowledgements

Stimulating discussions with Prof. N. Schwentner in a cooperation supported by the 'Deutsche Forschungsgemeinschaft' via a project on 'Analysis and control of ultrafast photoinduced reactions' (SFB 450) are gratefully acknowledged.

References

[1] R. Schinke, Photodissociation Dynamics, Cambridge University Press, Cambridge, 1993.
[2] E.J. Heller, J. Chem. Phys. 68 (1978) 2066.
[3] V.A. Apkarian, N. Schwentner, Chem. Rev. 99 (1999) 1481.
[4] R.B. Gerber, A.B. McCoy, A. Garcia-Vela, Annu. Rev. Phys. Chem. 45 (1994) 275.
[5] B. Schmidt, Chem. Phys. Lett. 301 (1999) 207.
[6] P. Ždánská, B. Schmidt, P. Jungwirth, J. Chem. Phys. 110 (1999) 6246.
[7] J. Manz, P. Saalfrank, B. Schmidt, J. Chem. Soc. Faraday Trans. 93 (1997) 957, see also http://www.rsc.org/is/journals/clic_rsc/net_4.htm.
[8] F.O. Ellison, J. Am. Chem. Soc. 85 (1963) 3540.
[9] I.H. Gersonde, H. Gabriel, J. Chem. Phys. 98 (1993) 2094.
[10] A.I. Krylov, R.B. Gerber, J. Chem. Phys. 106 (1997) 6574.
[11] V.S. Batista, D.F. Coker, J. Chem. Phys. 105 (1996) 4033.
[12] M.Y. Niv, R.B. Gerber, M. Bargheer, in preparation.
[13] G. Chaban, R.B. Gerber, M.V. Korolkov, J. Manz, M.Y. Niv, B. Schmidt, in preparation.
[14] M.D. Feit, J.A. Fleck Jr., A. Steiger, J. Comput. Phys. 47 (1982) 412.
[15] M. Hillery, R.F. O' Connell, M.O. Scully, E.P. Wigner, Phys. Rep. 106 (1984) 121.
[16] J.C. Tully, J. Chem. Phys. 93 (1990) 1061.